Chemical Science

Accepted Manuscript

This article can be cited before page numbers have been issued, to do this please use: P. Chen, B. Ding, H. Dou and X. Zhang, *Chem. Sci.*, 2026, DOI: 10.1039/D6SC02973F.

ROYAL SOCIETY OF CHEMISTRY

rsc.li/chemical-science

View Article Online
DOI: 10.1039/D6SC02973F

Fluoride-substituted $Li_{6.4}La_3Zr_{1.4}Ta_{0.6}O_{12}$ with Delocalized Electron-Share Accelerates Li^+ Desolvation Kinetics for High-voltage Lithium Metal Batteries

Peng Chen[a], Bing Ding[a,b,c], Hui Dou[a,b,c*], and Xiaogang Zhang[a,b,c]

[a]*Jiangsu Key Laboratory of Electrochemical Energy Storage Technologies, College of Materials Science and Technology, Nanjing University of Aeronautics and Astronautics, Nanjing 210016, P. R. China*

[b]*Shenzhen Research Institute, Nanjing University of Aeronautics and Astronautics, Shenzhen 518000, China*

[c]*National Key Laboratory of Mechanics and Control for Aerospace Structures, Institute for Frontier Science, Nanjing University of Aeronautics and Astronautics, Nanjing 210016, P.R. China*

**Corresponding author.*

E-mail address: dh_msc@nuaa.edu.cn (Hui Dou); azhangxg@nuaa.edu.cn (Xiaogang Zhang)

Keywords

delocalized-electron-shared • ion kinetic promoter • $Li(solvents)_x^+$ • theoretical simulation • high working voltage

Abstract

Metallic lithium is regarded as the ideal anode for the high-specific-energy battery. However, the $Li(solvents)_x^+$ formation in the liquid-state lithium metal batteries (LMBs) results in sluggish ion transport kinetics and continuous interface deterioration. Herein, an ion-kinetics promoter with delocalized-electron-share is designed to reduce the desolvation energy barrier, accelerate the interfacial lithium diffusion and achieve the stable interface. Specifically, the F-substituting $Li_{6.4}La_3Zr_{1.4}Ta_{0.6}O_{12}$ (named as $LLZTO_xF_y$) breaks the electron-confined state of the original metal-O (M-O) and

View Article Online
DOI: 10.1039/D6SC02973F

induces the electron-redistribution of the central metal sites, thus releasing more delocalized electrons. The relationships between charge transfer and ionic desolvation under the delocalized-electron-shared type promoter are deeply understood from theoretical calculations to in-situ characterizations. The F-substituting activates the O-M-F site activity of the $LLZTO_xF_y$, which enhance binding of C=O bond in solvent molecules to these sites, realizing a high Li^+ transference number (0.68). Consequently, the lithium-lithium symmetric cell based on $LLZTO_{0.95}F_{0.05}$@PP can stabilize cycling for 1400 h with a lower overpotential (7.3 mV). Meanwhile, the Li|$LLZTO_{0.95}F_{0.05}$@PP|$LiCoO_2$ full cell can retain a high specific capacity of 88.2% after 500th at 1.0 C under the high-voltage of 4.6 V. Therefore, this strategy contributes to achieving long-cycle stability of anodes in LMBs.

Introduction

Lithium (Li) metal has been considered as the promising anode for achieving high-energy-density rechargeable batteries due to the high specific capacity (3860 mA h g^{-1}) and the lowest electrochemical potential (-3.04 V vs. standard hydrogen electrode).[1-2] However, uncontrolled Li dendritic formation and continuous interfacial side reactions lead to short lifespan, and safety hazards as well, especially under high working voltage and high current density.[3] The formation of $Li(solvents)_x^+$ through the interactions between Li^+ and various solvents is considered as the principal hurdles for internal/interfacial Li^+ diffusion in the liquid-state Li metal batteries (LMBs), which ultimately causes the unbalanced interfacial electrochemistry and local Li^0 accumulation (Fig. 1a).[4-5] Worsely, the accumulated Li^0 will become incorporated by the metal lattice, forming the notorious Li dendrites.[6] That means, reconstructing the structure of $Li(solvents)_x^+$ can help to reduce the desolvation energy barrier and accelerate the rapid interfacial Li^+ transmission.[7-8] In spite of electrolyte engineering of tuning the local solvation shell, the desolvation energy barrier can be reduced by introducing ion-kinetics regulator, and a fast Li^+ transport channel can be constructed between the $Li(solvents)_x^+$ and Li anode, thereby promoting the Li^+ flux.[9-10]

Generally, the interfacial desolvation efficiency is related to the charge

View Article Online
DOI: 10.1039/D6SC02973F

distribution and transfer rate on the surface of the ion-kinetics regulators. The conventional ion-kinetics regulators with stable crystal structure induce electron-confined, decreasing the local charge separation and transport rate, and reducing the local activity (Fig. 1b).[11] As revealed in our previous work by replacing O atom with isoelectronic S atom, the heteroatoms-doping or heterojunctions construction could disrupt the original stable crystal structure and redistribute the local charge, providing more short-range and faster charge transfer channels.[12] However, the precise regulation of charge distribution and the development of advanced crystal structure design remain challenging. The theoretical proposal lacks further verification of the structure-activity relationships between microstructure and reaction kinetics.[13] Therefore, it is of great significance to known how to induce the delocalized charge redistribution by regulating atomic substitution and the reconstruction of more efficient and the shorter-range active sites in the microstructure.

Herein, we designed the delocalized-electron-shared (DES) ion kinetic promoter toward accelerating the desolvation kinetics by replacing the O atom with F atom. With lower valent electronic (-2 e^- vs. -1 e^-) and higher electronegativity (3.5 vs. 4.0), the unsaturated central metal sites are realized as the delocalized electron-shared (Fig. 1b).[12] As a demo, the construction of the F-substituted $LLZTO_xF_y$ DES ion kinetic promoter by fluorination is designed on the fast Li^+ conductor $Li_{6.4}La_3Zr_{1.4}Ta_{0.6}O_{12}$ (LLZTO), serving as the polypropylene (PP) separator modification layer to effectively regulate the interfacial $Li(solvents)_x^+$ desolvation, Li^+ diffusion and nucleation behaviors (Fig. S1). Consistent with theoretical calculations and in-situ Fourier transform infrared spectroscopy (FTIR), the reconstruction of delocalized electric active sites contributes to the break of electron-confined state of the original O-metal-O (O-M-O), building up a stronger local electric field (O-M-F) to anchor the anions and solvents, enhancing the stability of Li anode. Thus, the Li||Li symmetric cell with $LLZTO_{0.95}F_{0.05}$@PP cycles stably for over 900 h without short circuit, at 0.5 mA cm^{-2}, 0.5 mAh cm^{-2}. Notably, even when coupled with high-voltage $LiCoO_2$ (LCO, 3.0-4.6 V, 1.0 C = 220 mAh g^{-1}) cathodes, the Li|$LLZTO_{0.95}F_{0.05}$@PP|LCO full cell retains a specific capacity of 100 mAh g^{-1} after 250 cycles at 4.0 C. Moreover, the

Li|LLZTO$_{0.95}$F$_{0.05}$@PP|LCO cell maintains a capacity retention rate of 94.5% after 120 cycles at 0.5 C under 0°C. Therefore, the LMBs fabricated using the LLZTO$_x$F$_y$ DES ion kinetic promoter exhibited a superior cycle life.

Results and Discussion

The regulation of the electronic structure and transport path in the promoter is important for electrochemical performance.[14] With the local delocalized electron-shared states, more free electrons can participate in the reactions for high desolvation efficiency.[15] Based on these principles, we established models of LLZTO with F atom-substitution and used density functional theory (DFT) calculations to investigate the electron delocalization effect of kinetic promoter to achieve rapid Li diffusion. The charge density difference in Fig. 1c indicates that the metastable M-O$_3$-F structure has the efficient interfacial separation and transfer compared with the balanced M-O$_4$ structure in LLZTO, thereby building atomic-level electron transport channels.[12] Moreover, substitution of F (with a valence electron of -0.88 eV) for O (-1.42 eV) alters the valence charge distribution of both the central metal atoms, promoting more free electrons to achieve the delocalized electron-shared (Fig. 1d). The projected density of states in Fig. 1e and S2 reveal that LLZTO-F exhibits a non-zero density of states at the Fermi level and the electrons occupy spin-up states, indicating that the F atom-substitution enhances the local electrons transport of LLZTO. The models for Li^+, anions, and solvents on the LLZTO-F and LLZTO had been established and the relevant adsorption energy, desolvation energy barrier, and surface diffusion energy barrier had been also calculated to evaluate the comprehensive performance of DES ion kinetic promoter.[16] As shown in Fig. 1f and S3, the adsorption energy of PF_6^- anion on the LLZTO-F and LLZTO are -7.16 eV and -4.14 eV, respectively, indicating that the anions can be anchor on the DES ion kinetic promoter and the dissociation of Li salts can be accelerated. Meanwhile, with the introduction of F atom, the adsorption energies of solvents, such as ethylene carbonate (EC) and diethyl carbonate (DEC), on the LLZTO-F are -0.22 eV and -0.72 eV, respectively, which are higher than those on the LLZTO (-0.18 eV and -0.22 eV).[17] Besides, the LLZTO-F has a lower desolvation energy

View Article Online
DOI: 10.1039/D6SC02973F

barrier (1.95 eV) than that of LLZTO (2.13 eV), which enables the rapid desolvation of Li(solvent)$_x^+$ and avoids the local accumulation of Li^+ (Fig. 1g).[7, 17-18] With the lattice distortion and the augmentation of active sites caused by F-substitution, Li rapidly migrates on the surface of LLZTO-F (0.80 eV), thereby avoiding Li dendrites growth (Fig. 1h). Thus, the calculations strongly suggest that introducing the DES ion kinetic promoter increases the interfacial/internal Li^+/Li^0 diffusion rates and balances the interfacial electrochemistry, thereby achieving satisfied electrochemical performance of LMBs.[19-20]

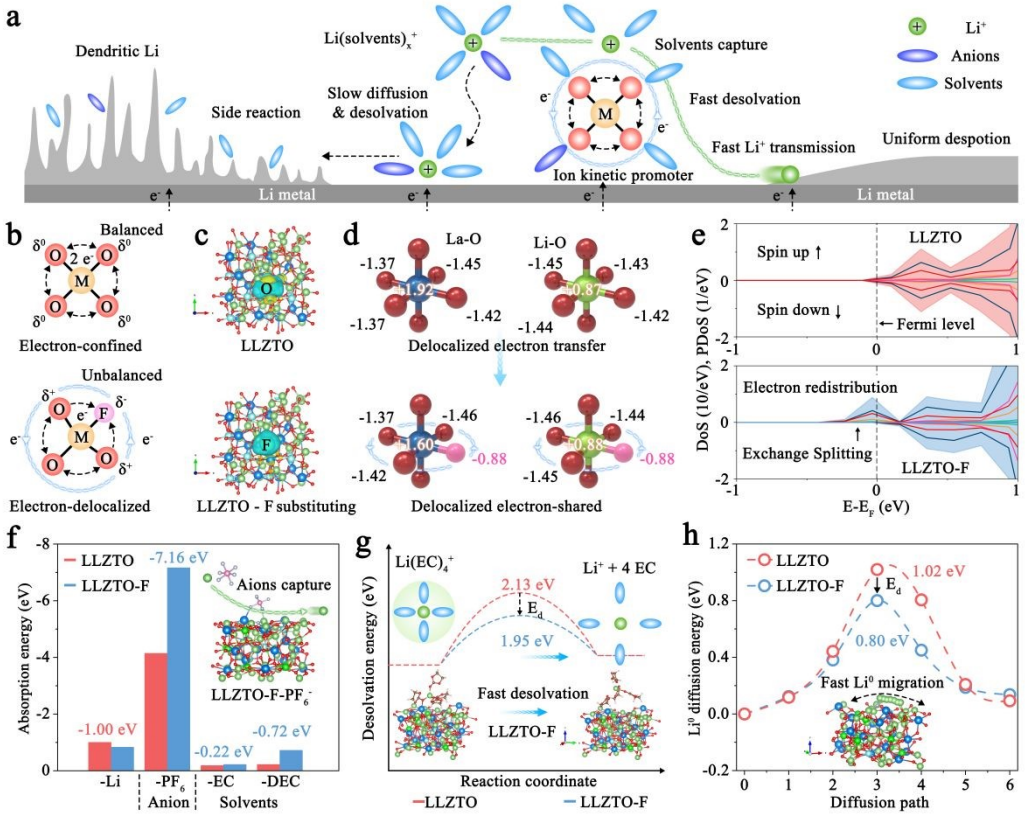

Fig. 1. (a) The interfacial de-solvation evolution of Li(solvent)$_x^+$ species and Li^+ deposition with/without ion kinetic promoter. (b) Schematic diagram of electron-confined and electron-delocalized ion kinetic promoter. (c) Charge density difference of LLZTO and LLZTO-F. (d) Valence electron number of La-O and Li-O with/without F-substituting. (e) Partial density of states. (f) Absorption energy of Li, PF_6, and solvents on LLZTO and LLZTO-F. (g) Desolvation energy barrier and (h) Li^0 diffusion energy barrier on LLZTO and LLZTO-F.

In our treatment (Fig. 2a), pristine LLZTO was exposed to HF vapor by heating NH_4F to transform into $LLZTO_xF_y$ DES ion kinetic promoter.[21] By regulating the ratio between NH_4F and LLZTO, the atomic O/F ratio in the $LLZTO_xF_y$ is adjusted, inducing local charge redistribution and constructing DES ion kinetic promoter with higher activity. After the fluorination, a F signal was detected and gradually increased in X-ray photoelectronic spectroscopy (XPS, Fig. S5) with the O signal progressively decreases, indicating the successful formation of $LLZTO_xF_y$. For simplification, these optimized samples with the gradual conversion are identified as $LLZTO_{1.00}$, $LLZTO_{0.95}F_{0.05}$, $LLZTO_{0.91}F_{0.09}$, and $LLZTO_{0.71}F_{0.29}$ according to the XPS. As shown in Fig. 2b, atomic F preferentially replaces the O site adjacent to La to form the La-F. And then, with the increase of F content, the characteristic peaks of Zr-F and Li-F gradually enhance while the Li-O decreases (Fig. S6a). Accordingly, we observe the characteristic peaks of Li 1s, Zr 3d, and Ta 4f shift towards the direction of high binding energy, indicating that the bonding strength are enhanced due to the formed M-F bond in $LLZTO_{0.71}F_{0.29}$, achieving strong separation of local charges-holes and improving interfacial charge transfer rate (Fig. S6a-d).[22] While, the characteristic peak of La 3d shifts towards lower binding energies, indicating that La site gains electrons and forms the unsaturated site metal. This result was also verified by O 1s (Fig. 2c). The components of $LLZTO_xF_y$ was further investigated by X-ray diffraction (XRD). The atomic F-substitution in $LLZTO_{0.95}F_{0.05}$ did not induce lattice distortion, effectively ensuring the stability of the DES ion kinetic promoter (Fig. 2d). With the O/F ratio reach approximately 9:1, the characteristic peak of LaF_3 (45.0°) emerges in $LLZTO_{0.91}F_{0.09}$. Therefore, it can be inferred that F preferentially substitutes the O site adjacent to La, thereby constructing a metastable F-La-O_3 structure. With the further substitution of the F atom, distinct peaks of Li_4ZrF_8 and LaF_3 emerge in $LLZTO_{0.71}F_{0.29}$. Although both slightly soluble LaF_3 and Li_4ZrF_8 contribute to stabilizing the Li anode, their formation is generally regarded as detrimental to interfacial stability, as it leads to the collapse of the $LLZTO_xF_y$ structure and defect increase.[23-24]

The microstructure of $LLZTO_xF_y$ DES ion kinetic promoter was analyzed using scanning electron microscopy (SEM) and high-resolution transmission electron

View Article Online
DOI: 10.1039/D6SC02973F

microscopy (HRTEM). As shown in Fig. S7, with the substitution of F atoms, $LLZTO_{1.00}$ gradually transforms from square particles to spherical particles ($LLZTO_{0.71}F_{0.29}$) with low surface energy, which was also preliminarily verified by elemental analysis (Fig. S8-11).[25] The HRTEM further characterized the phase evolution of $LLZTO_xF_y$. The lattice fringes and diffraction rings of $LLZTO_{0.95}F_{0.05}$ are more distinct than that in $LLZTO_{1.00}$ due to the repair of intrinsic defects by F-substitution. Meanwhile, the lattice interlacing on the surface of $LLZTO_{0.95}F_{0.05}$ indicates the presence of multiple phases corresponding to the XRD. As shown in Fig. 2e, the lattice spacings are 0.310, 0.286, and 0.211 nm, which is consistent with the (221), (222) planes of LaF_3 and the (512) plane of $LLZTO_{1.00}$, respectively. As the substitution of F increases gradually, the substantial formation of slightly soluble LaF_3 leads to structural degradation in both $LLZTO_{0.91}F_{0.09}$ and $LLZTO_{0.71}F_{0.29}$, which will cause the deactivation of the ion kinetic promoter during the electrochemical process (Fig. 2f and S12-14). Therefore, atomic-level F-substitution is beneficial to improve the structural stability and achieve persistent interfacial ion transport regulation.

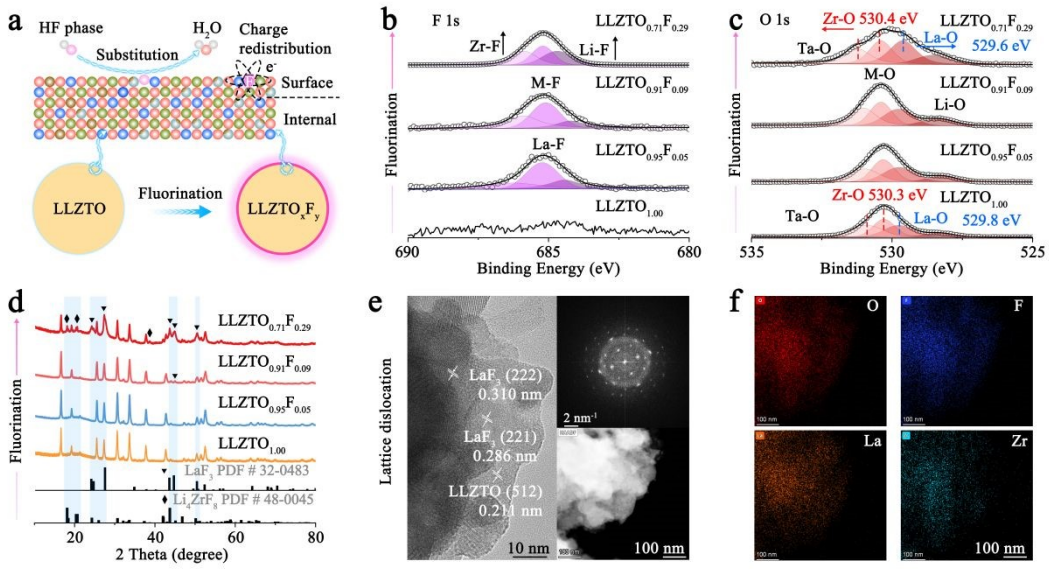

Fig. 2. (a) Schematic illustration of vapor-phase fluoride treatment. The comparisons of (b) F 1s, (c) O 1s XPS spectra, and (d) XRD of $LLZTO_xF_y$. (e) HRTEM images and (f) elemental mappings of the $LLZTO_{0.95}F_{0.05}$.

Separator with micro-level pores is crucial for transmitting ions in liquid-state

LMBs (Fig. S15). However, the Li(solvent)$_x^+$ can also pass through the micron pores of separator freely.[18] Therefore, the LLZTO$_x$F$_y$ was coated on the commercial PP separator (Fig. S16) to promote rapid desolvation and accelerate interfacial ion transport. Moreover, the LLZTO$_x$F$_y$ modification layer improves the electrolyte wettability, compared with the PP separator (10.9° vs. 26.6°), which helps to reduce the interface resistance (Fig. S17). Besides, the introduction of atomic F induces the local charges redistribution, anchoring the anions and solvents, thus releasing more free Li^+ (Fig. S18), which is consistent with the theoretical calculation results. Moreover, the introduction of LLZTO$_x$F$_y$ modification layer contributes to construct composite separator with better physical/chemical stability (Fig. S19).[26]

Symmetric cells were assembled and evaluated the regulation of interfacial ion desolvation and transport nucleation during the electrochemical process.[27] Fig. 3a and Fig. S20 show that Li||Li symmetric cell with LLZTO$_{0.95}$F$_{0.05}$@PP exhibits the higher Li^+ transference number (t_{Li+} = 0.68) than that of LLZTO$_{1.00}$@PP (0.58) and PP (0.32) due to the high anion adsorption energy. With the low desolvation energy barrier and interfacial ion migration energy barrier, the LLZTO$_{0.95}$F$_{0.05}$@PP-based Li||Li symmetrical cell exhibits a critical current density of 7.5 mA cm^{-2}, much higher than that with LLZTO$_{1.00}$ (6.0 mA cm^{-2}) and PP (5.0 mA cm^{-2}, Fig. 3b and S21). On the contrary, excessive F-substitution induces lattice distortion and causes the structural collapse of the LLZTO$_{0.95}$F$_{0.05}$ due to the dissolution of LaF_3, resulting in continuous interface deterioration and local dendritic Li growth, ultimately causing the short circuit (Fig. S22).[28] The rate performance shown in Fig. 3c indicates that the introduction of atomic F contributes to reducing the nucleation overpotential due to the reduction of interfacial Li nucleation energy barrier. Among them, the initial electroplating polarization voltages of LLZTO$_{0.95}$F$_{0.05}$@PP-based Li||Li symmetrical cell at 0.1, 0.2, 0.4, 0.5, 1.0, 2.0 and 4.0 mA cm^{-2} are 23.0, 24.6, 37.0, 40.7, 71.4, 119.3 and 201.7 mV, respectively. When the current density recovered to 0.1 mA cm^{-2}, a low polarization potential of 6.8 mV is still retained at 213 h without short circuit (Fig. S23). Moreover, at a current density of 0.1 mA cm^{-2}, 0.5 mA cm^{-2}, and the capacities of 0.1 mAh cm^{-2}, 0.5 mAh cm^{-2} were selected to investigate the long cycle stability of the LLZTO$_x$F$_y$

View Article Online
DOI: 10.1039/D6SC02973F

DES ion kinetic promoter. The $LLZTO_{0.95}F_{0.05}$@PP can stably plate/strip for 1400 h with low over-potential (7.3 mV) at 0.1 mA cm^{-2} (Fig. 3d and S24). Even under the current density of 0.5 mA cm^{-2}, the $LLZTO_{0.95}F_{0.05}$-based symmetrical cell achieves uniform interfacial Li atom nucleation for over 900 h (Fig. 3e and S25). By contrast, the continuous interface deterioration and the local Li nucleation lead to a short circuit in that on $LLZTO_{1.00}$@PP (650 h) and $LLZTO_{0.91}F_{0.09}$@PP (880 h).

To further reveal the role of $LLZTO_xF_y$ DES ion kinetic promoter in interfacial regulation, it is crucial to clarify the evolution of the Li nucleation morphology during electrodeposition. The Li|$LLZTO_xF_y$@PP|Li symmetric cells were tested under 25 cycles and the composition changes of the cycled-Li anodes were been investigated (Fig.3f and S26). As shown in Fig. 3f-g, S27a-b, the delocalized electron-shared layer decrease the interfacial ion migration energy barrier, accelerating the rapid interfacial Li^+/Li^0 migration for achieving uniform Li^0 nucleation.[29-30] By contrast, $LLZTO_{1.00}$, with large desolvation energy barrier and Li^0 migration energy barrier, induces Li^0 nucleation on the (200) crystal plane and vertical Li dendrites growth, which is manifested as nanoparticles in the SEM image (Fig. S27b1).[31] Meanwhile, during the plating/stripping, the structural collapse of $LLZTO_{0.71}F_{0.29}$ leads to continuous interface deterioration with dendrites growth, ultimately resulting in continuous increase of polarization potential and substantial Li dendrites growth (Fig. 3g and S27b4). The structural evolution of solid electrolyte interphase (SEI) layer in Li anode during electrochemical processes is critical for regulating interfacial ion transport and Li deposition behavior. The component distribution of SEI was further confirmed by time-of-flight secondary ion mass spectrometry (TOF-SIMS). For the SEI on the cycled Li metal protecting by the $LLZTO_{1.00}$ and $LLZTO_{0.71}F_{0.29}$, the dense LiF layer with high interfacial Li^+ diffusion energy barrier forms on the surface of SEI (Fig. 3h).[32] Conversely, the distribution of LiF and Li_2O in Fig. 3h and S28 indirectly demonstrates that interfacial degradation of Li anode and electrolyte decomposition can be inhibited with the anchoring effect of $LLZTO_{0.95}F_{0.05}$.[33] Meanwhile, the content and distribution of the CH_2O^- further corroborates the aforementioned viewpoint.[34] Therefore, atomic F-substitution will induce the charge-redistribution of the central La atoms, thereby

enhancing the local charge transport of the $LLZTO_{0.95}F_{0.05}$, and thus achieving rapid interfacial ion transport and uniform Li^0 deposition.

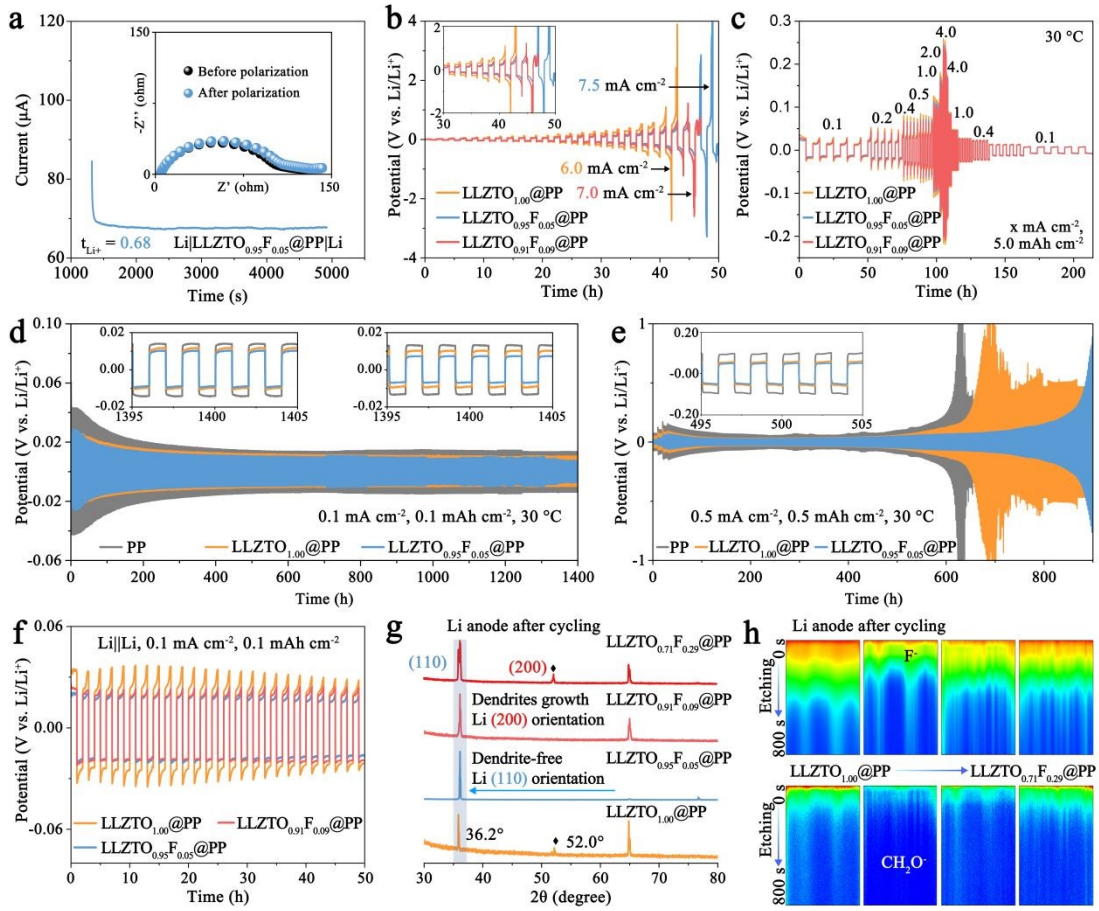

Fig. 3. (a) Current-time curves of the Li|$LLZTO_{0.95}F_{0.05}$@PP|Li symmetric cell with a perturbation of 10 mV. (b) Critical current density values and (c) rate performance of Li||Li symmetric cells at 0.1~4.0 mA cm^{-2}, 5.0 mAh cm^{-2}. Galvanostatic voltage profiles of Li||Li symmetric cells using different $LLZTO_xF_y$@PP at (d and f) 0.1 mA cm^{-2}, 0.1 mAh cm^{-2} and (e) 1.0 mA cm^{-2}, 1.0 mAh cm^{-2}, at 30 °C.(g) XRD and (h) TOF-SIMS of the Li metal within Li|$LLZTO_xF_y$@PP|Li symmetric cells after cycling.

The high-voltage full cells were assembled to investigate the electrochemical performance of DES ion kinetic promoter.[35-36] The cyclic voltammogram (CV) in Fig 4a shows that the Li|$LLZTO_{0.95}F_{0.05}$@PP|LCO exhibits high redox peak current and low redox voltage (281.3 mV) at 0.1 mV s^{-1}. Meanwhile, the polarization voltage of the oxidation and reduction peaks of the Li|$LLZTO_{0.95}F_{0.05}$@PP|LCO cell are only 53.3 mV

View Article Online
DOI: 10.1039/D6SC02973F

and 60.2 mV, respectively, which are much lower than those of the cells with $LLZTO_{1.00}$ (83.3 mV, 70.0 mV) and PP (113.6 mV, 83.0 mV), from 0.2 mV s^{-1} to 1.0 mV s^{-1} (Fig. 4b and S29). This further indicates the $LLZTO_{0.95}F_{0.05}$ DES ion kinetic promoter contributes to enhance the interfacial Li^+ transport and enables rapid Li^0 migration on the surfaces of the anode and cathode (Fig. 4c). The initial specific capacities of the Li|$LLZTO_{0.95}F_{0.05}$@PP|LCO cell at 0.1, 0.2, 0.5, 1.0, 2.0, 3.0, and 4.0 C are 207.6, 207.0, 197.6, 185.6, 168.1, 154.2, and 143.6 mAh g^{-1}, respectively (Fig. 4d-e and S30). While, it still maintains a high specific capacity of 198.8 mAh g^{-1} with the current density restored to 0.2 C, which is much higher than that of the Li||LCO with PP (176.1 mAh g^{-1}) and LLZTO@PP (187.5 mAh g^{-1}) at 36th cycles. Meanwhile, with the improved interfacial ion transport rate and interface stability, the Li|$LLZTO_{0.95}F_{0.05}$@PP|LCO cell retains a high specific capacity of 88.2% after 500 cycles at 1.0 C and still exhibits a high specific capacity of 100 mAh g^{-1} after 250 cycles at 4.0 C (Fig. 4f-g). Moreover, the Li|$LLZTO_{0.95}F_{0.05}$@PP|LCO cell maintains a capacity retention rate of 94.5% after 120 cycles at 0.5 C, further proving that the DES ion kinetic promoter can de-solvate and accelerate interfacial ion transport even at low temperature (Fig. 4h).[37] Therefore, the $LLZTO_{0.95}F_{0.05}$ DES ion kinetic promoter accelerates the desolvation kinetics to build a long-lasting stable Li metal anode.

View Article Online
DOI: 10.1039/D6SC02973F

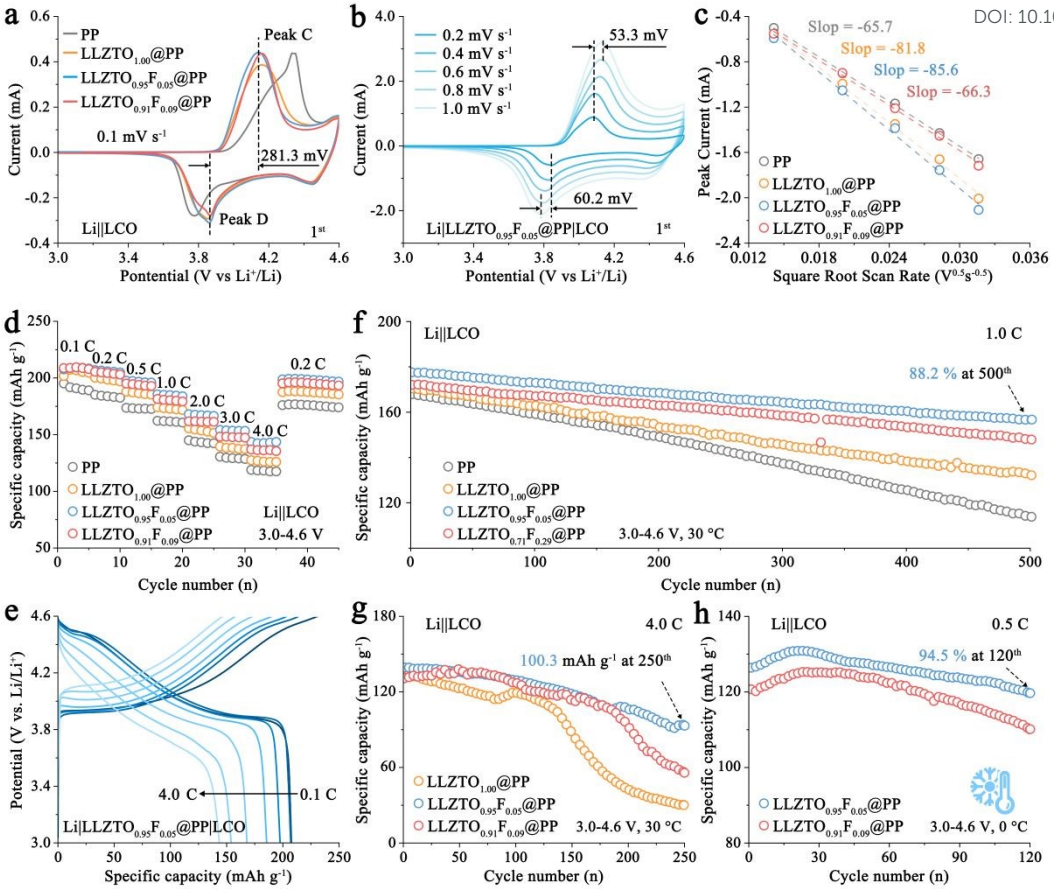

Fig. 4. (a-b) CV curves of Li|LLZTO$_x$F$_y$@PP|LCO. (c) Plots of logarithm peak current versus logarithm scan rates. (d-e) Rate capability and cycling performance of Li||LCO cells with different LLZTO$_x$F$_y$@PP at (f) 1.0 C, (g) 4.0 C, and (h) 0.5 C.

To understand the key factor of DES ion kinetic promoter in enhancing the performance of LMBs, in-situ FTIR was employed to investigate the solvation structure evolution of Li(solvent)$_x^+$ on the LLZTO$_{0.95}$F$_{0.05}$. Fig. 5a reveals that the solvation structure of Li(solvent)$_x^+$ remained unchanged. By contrast, distinct C=O (1750~1600 cm^{-1}) and CH$_2$/CH$_3$ (1600~1400 cm^{-1}) infrared characteristic peaks can be detected on the LLZTO$_{0.95}$F$_{0.05}$@PP separator (Fig. 5b).[38-39] Furthermore, under the applied electric field, the peak of C=O and CH$_2$/CH$_3$ are increased, which indicates that solvent molecules (EC and DEC) have been captured by LLZTO$_{0.95}$F$_{0.05}$, thereby releasing additional free Li$^+$ and accelerating interfacial Li$^+$ transport kinetics. While, due to the inherently limited desolvation kinetics of LLZTO$_{1.00}$, solvents will still shuttle freely under the electric field (Fig. S31). Subsequently, in-situ electrochemical impedance

View Article Online
DOI: 10.1039/D6SC02973F

spectroscopy (EIS) and distribution of relaxation times (DRT) fitting were carried out.[40] The poor interfacial contact between the PP separator and electrolyte induces the high interfacial charge-transfer resistance, leading to elevated contact resistance (10^{-6} to 10^{-5} s) and inherent internal resistance (10^{-5} to 10^{-4} s, Fig. 5c-d and S32a-b). Concurrently, the sluggish ion transport and a high interfacial desolvation energy barrier of $Li(solvent)_x^+$, resulting in significant interfacial transmission impedance (10^{-4} to 10^{-3} s) for Li|PP|Li symmetric cell. Conversely, $LLZTO_{0.95}F_{0.05}$ facilitates rapid desolvation of interfacial $Li(solvent)_x^+$, promoting efficient Li^+ diffusion and transport (Fig. 5e-f and S32c-d).

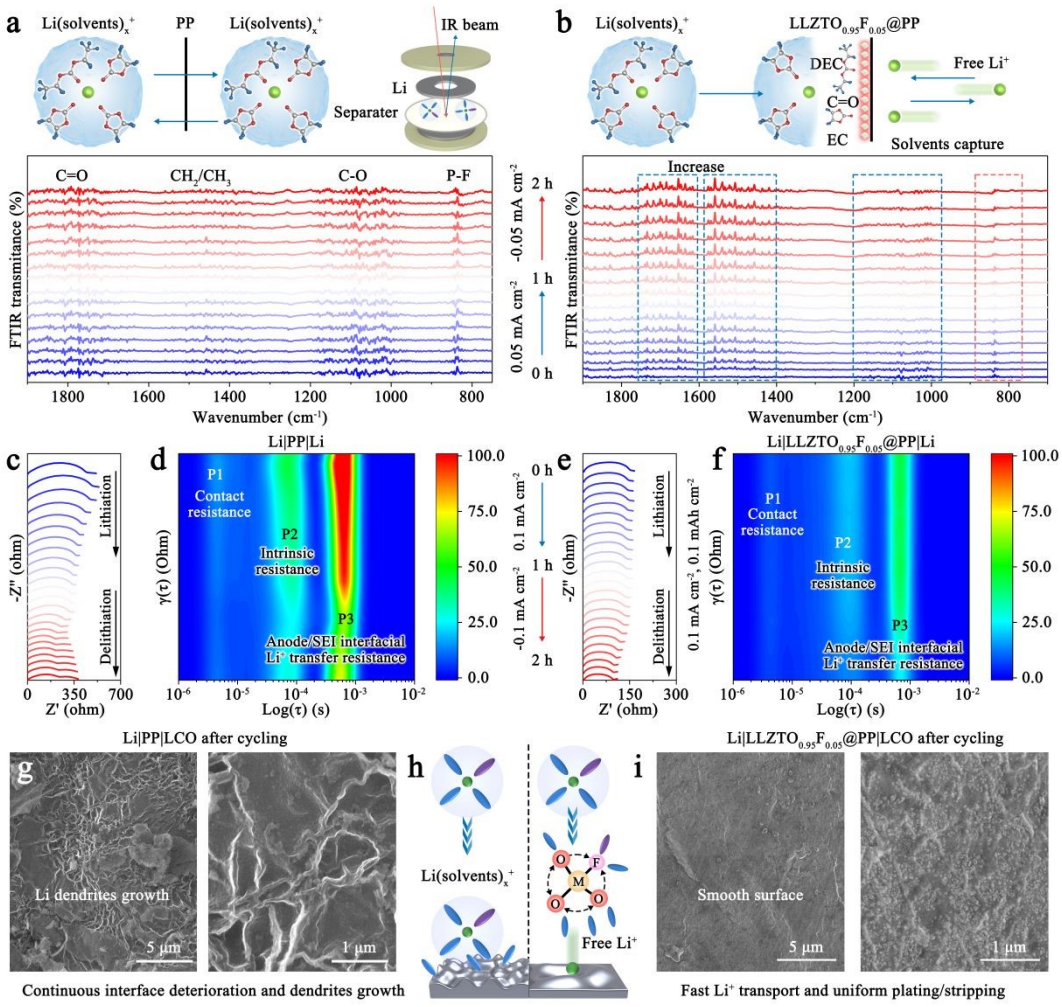

Fig. 5. (a-b) In-situ FTIR spectroscopy reveals the solvation structure evolution of $Li(solvent)_x^+$ in Li||Li symmetric cells. In-situ (c) EIS and (d) DRT of Li|PP|Li. In-situ (e) EIS and (f) DRT of Li|$LLZTO_{0.95}F_{0.05}$@PP|Li. (g and i) SEM images of cycled Li anode in Li||LCO at 20th under 0.2 C. (h) Schematic diagram of the desolvation

View Article Online
DOI: 10.1039/D6SC02973F

mechanism of DES ion kinetic promoter.

To further elucidate the working mechanism of $LLZTO_{0.95}F_{0.05}$ DES ion kinetic promoter, cycled Li anodes were disassembled and characterized. Fig. 5g-h demonstrates that the coexistence of free solvent molecules and sluggish interfacial Li^+ transport degrade the Li metal, promoting the formation of sheet-like Li dendrites.[27] By contrast, with the introduce of $LLZTO_{0.95}F_{0.05}$ DES ion kinetic promoter, the Li deposition occurred via fine-grained growth, contributing to the long-cycling stability (Fig. 5i). Consequently, this DES ion kinetic promoter-mediated desolvation strategy effectively promotes the long-cycle stability of LMBs.

Conclusion

In this work, a new concept of delocalized-electron-shared ion kinetic promoter is proposed to accelerate the desolvation of $Li(solvent)_x^+$. As a proof-of-concept model, various $LLZTO_xF_y$ DES ion kinetic promoters with different degrees of fluorination are systematically fabricated and investigated. Theoretical calculations reveal that F-substitute disrupts the equilibrium state of the $M\text{-}O_4$ structure, inducing charge redistribution on the $M\text{-}O_3\text{-}F$ and facilitating delocalized electron sharing. In-situ FTIR and electrochemical experiments corroborate that the $LLZTO_{0.95}F_{0.05}$ DES ion kinetic promoter effectively anchors solvent molecules and anions, especially under the applied electric field, releasing free Li^+ and accelerating interfacial Li diffusion/nucleation kinetics. Consequently, the $Li|LLZTO_{0.95}F_{0.05}@PP|Li$ symmetrical cell can cycle for over 900 h under 0.5 mA cm^{-2} without short circuit. The Li||LCO with $LLZTO_{0.95}F_{0.05}@PP$ can still maintain a capacity retention rate of 94.5% at 120^{th} at 0.5 C under 0°C. Our work has pointed out a new way to regulate the local electronic density, generating more active sites to accelerate interfacial kinetics and realizing the practical LMBs.

Experimental Section

Detailed experimental methods can be found in the Supporting Information.

View Article Online
DOI: 10.1039/D6SC02973F

Author Contributions

Peng Chen conceived the idea, conducted the materials preparation, battery-related experiments, simulations, and prepared the draft manuscript. Bing Ding, and Xiaogang Zhang participated in discussions. Hui Dou and Xiaogang Zhang contributed to manuscript editing, funding acquisition, and conceptualization.

Conflicts of interest

There are no conflicts to declare.

Data availability

All the data supporting this article have been included in the main text and the supplementary information.

Acknowledgements

This work was supported by the National Natural Science Foundation Funded Project (52372199), National Key Research and Development Program of China (2023YFB2405800), Shenzhen Longhua Science and Technology Innovation Special Funding Project (Industrial Sci-Tech Innovation Center of Low-Altitude Intelligent Networking), Shenzhen Science and Technology Program (JCYJ20250604190043054), Leading Edge Technology of Jiangsu Province (BK20232022, BK20220009). The authors thank for the tests supported from Center for Microscopy and Analysis, Nanjing University of Aeronautics and Astronautics.

Reference

[1] Q. Kang, Z. Zhuang, Y. Li, Y. Zuo, J. Wang, Y. Liu, C. Shi, J. Chen, H. Li, P. Jiang, X. Huang, Nano Res. **2023**, 16, 9240–9249.

[2] Y. Zang, P. Peng, F. Pei, R. H. Li, L. Wu, D. Q. Lu, Y. Zhang, K. Huang, Y. Shen, Y. H. Huang, Y. Q. Lan, Natl. Sci. Rev. **2025**, 12, nwae443.

[3] T. Wang, Y. Li, J. Zhang, K. Yan, P. Jaumaux, J. Yang, C. Wang, D. Shanmukaraj, B. Sun, M. Armand, Y. Cui, G. Wang, Nat. Commun. **2020**, 11, 5429.

[4] J. Dong, X. Cheng, H. Yang, H. Li, H. Liu, L. Jia, Y. Zhang, Q. Guan, J. Jia, F. Wu, J. Zhang, M. Liu, H. Lin, J. Wang, Adv. Mater. **2025**, 37, 2501079.

[5] Q. He, Z. Deng, S. Miao, Y. Jia, J. Peng, P. Xia, C. Xu, Q. Tang, X. Zhang, T. Tan, G. Zhu, K. Wu, Y. Fang, Y. Zhang, W. Cai, Energy Environ. Sci. **2025**, 18, 9093–9104.

[6] J. Xiao, Science. **2019**, 366, 426–427.

[7] Y. Lin, J. Wang, X. Zhang, X. Cheng, Q. Zhuang, J. Zhang, Q. Guan, Y. Wang, C. Shen, H. Lin, L. Zhan, L. Ling, Y. Zhang, Adv. Funct. Mater. **2025**, 35, 2501496.

[8] S. Li, K. Huang, L. Wu, D. Xiao, J. Long, C. Wang, H. Dou, P. Chen, X. Zhang, Chem. Sci. **2023**, 14, 10786–10794.

[9] Z. Hu, Z. Han, H. Liu, X. Jiang, K. Bai, S. Huang, Z. Yang, M. Ye, Y. Tang, Y. Zhang, X. Liu, Z. Wen, H. S. Park, C. C. Li, J. Am. Chem. Soc. **2025**, 147, 46632–46641.

[10] R. Xu, A. Hu, W. Xu, W. Yang, F. Li, Y. Li, Y. Mu, L. Zeng, J. Long, S. Chen, Angew. Chem. Int. Ed. Engl. **2025**, 64, e202513321.

[11] Y. He, D. Xiong, M. Chen, W. Zhang, S. Liu, Y. Ye, M. Wang, Y. Chen, Q. Tang, X. Peng, C. Wang, H. Zhan, H. Liu, M. Liu, J. Su, H. Shu, J. Wang, X. Wang, Angew. Chem. Int. Ed. Engl. **2025**, 64, e202512168.

[12] P. Chen, T. Wang, D. He, T. Shi, M. Chen, K. Fang, H. Lin, J. Wang, C. Wang, H. Pang, Angew. Chem. Int. Ed. Engl. **2023**, 62, e202311693.

[13] B. Wu, Z. Chen, Y. Ye, J. Z. Y. Seow, D. Mandler, A. Fisher, D. Wang, S. Guo, Z. J. Xu, Chem. Soc. Rev. **2026**, 55, 114–143.

[14] L. Chen, X. Guan, Z. Yao, S. Hayama, M. A. V. Spronsen, B. Karagoz, G. Held, D. G. Hopkinson, C. S. Allen, J. Callison, P. J. Dyson, F. R. Wang, Nat. Commun. **2025**, 16, 9412.

[15] J. Zhang, L. Pan, L. Jia, J. Dong, C. You, C. Han, N. Tian, X. Cheng, B. Tang, Q. Guan, Y. Zhang, B. Deng, L. Lei, M. Liu, H. Lin, J. Wang, Nano Lett. **2025**, 25, 3756–3765.

[16] J. Wang, J. Zhang, Y. Zhang, H. Li, P. Chen, C. You, M. Liu, H. Lin, S. Passerini, Adv. Mater. **2024**, 36, 2402792.

[17] B. Yang, Y. Wang, R. Zheng, W. Yang, Y. Li, T. Li, K. Li, A. Hu, J. Long, S. Ding, Angew. Chem. Int. Ed. Engl. **2025**, 64, e202508486.

[18] J. Qin, F. Pei, R. Wang, L. Wu, Y. Han, P. Xiao, Y. Shen, L. Yuan, Y. Huang, D. Wang, Adv. Mater. **2024**, 36, 2312773.

[19] Q. Kang, Z. Zhuang, Y. Liu, Z. Liu, Y. Li, B. Sun, F. Pei, H. Zhu, H. Li, P. Li, Y. Lin, K. Shi, Y. Zhu, J. Chen, C. Shi, Y. Zhao, P. Jiang, Y. Xia, D. Wang, X. Huang, Adv. Mater. **2023**, 35, 2303460.

[20] P. Chen, P. Guo, W. Guo, B. Ding, H. Dou, X. Zhang, J. Energy Chem. **2025**, 110, 363–371.

[21] X. Zhao, P. Zang, T. Liu, Y. Jiang, J. Zhang, Y. Tang, B. Li, M. Xue, W. Zhang, Z. Zhang, W. Guo, Science. **2024**, 385, 433–438.
[22] C. He, L. Yang, J. Wang, T. Wang, J. Ju, Y. Lu, W. Chen, Carbon Energy. **2024**, 6, e573.
[23] W. Lin, Q. Gao, Y. Zhang, F. Zhang, Z. Huang, Q. Kang, Y. Liao, L. Wu, S. Hao, Y. Ren, F. Pei, Y. Huang, J. Am. Chem. Soc. **2025**, 147, 43655–43665.
[24] Q. Xu, T. Li, Z. Ju, G. Chen, D. Ye, G. I. N. Waterhouse, Y. Lu, X. Lai, G. Zhou, L. Guo, K. Yan, X. Tao, H. Li, Y. Qiu, Nature. **2025**, 637, 339–346.
[25] X. Zhang, J. Li, T. Wang, Y. Gong, J. Zhou, Nat. Commun. **2025**, 16, 5781.
[26] S. Cai, X. Du, X. Gao, C. Zhao, C. Cheng, R. Lin, X. Yang, D. Luo, R. Sun, Z. Chen, Nano Energy. **2025**, 140, 111031.
[27] Q. Yang, C. Wang, L. Song, Y. Zhang, Z. Shen, W. Cai, Y. Song, Angew. Chem. Int. Ed. Engl. **2025**, 64, e202415078.
[28] K. Yan, Z. Lu, H.-W. Lee, F. Xiong, P.-C. Hsu, Y. Li, J. Zhao, S. Chu, Y. Cui, Nat. Energy. **2016**, 1, 16010.
[29] G. Yang, Y. Li, C. Zhang, J. Wang, Y. Bai, C. Y. J. Lim, M. F. Ng, Z. Chang, S. Kumar, Z. Sofer, W. Liu, Z. W. Seh, Nano Lett. **2022**, 22, 9138–9146.
[30] Q. Yang, S. Shen, Z. Han, G. Li, D. Liu, Q. Zhang, L. Song, D. Wang, G. Zhou, Y. Song, Adv. Mater. **2024**, 36, 2405790.
[31] Z. Sun, Y. Wang, S. Shen, X. Li, X. Hu, M. Hu, Y. Su, S. Ding, C. Xiao, Angew. Chem. Int. Ed. Engl. **2023**, 62, e202309622.
[32] S. Li, S. Fang, H. Dou, X. Zhang, ACS Appl. Mater. Interfaces. **2019**, 11, 20804–20811.
[33] X. Chen, M. Jiang, X. Du, X. Gao, K. Feng, Y. Liu, X. Yang, R. Sun, D. Luo, Z. Chen, Adv. Energy Mater. **2025**, 15, 2502589.
[34] H. Ji, J. Xiang, Y. Li, M. Zheng, L. Yuan, Y. Liao, L. Du, Z. Li, Z. Xie, K. Huang, X. Lin, Z. Xie, Y. Shen, M. Chen, T. Li, G. Feng, Y. Sun, L. Qie, H. Li, F. Zhang, R. Guo, X. Feng, W. Chen, X. Ai, J. Lu, Y. Huang, Nature. **2025**, 643, 1255–1262.
[35] Z. Hao, X. Liu, Y. Li, J. Liu, H. Li, L. Wang, G. Yang, J. Ma, Adv. Energy Mater. **2025**, 15, 2502242.
[36] X. Yang, Y. Lin, S. Tang, Y. Zhou, X. Huang, W. Song, W. Yang, Y. Yang, Energy Storage Mater. **2025**, 81, 104473.
[37] P. Chen, T. Huang, T. Wei, B. Ding, H. Dou, X. Zhang, Adv. Funct. Mater. **2025**, 35, 2420351.
[38] J. Wang, J. Zhang, X. Cheng, Y. Zhang, H. Li, Q. Guan, F. Wu, H. Li, D. Wang, M. Liu, Y. Zhang, Q. Xiao, S. Passerini, H. Lin, J. Am. Chem. Soc. **2025**, 147, 44633–44651.
[39] H. Luo, X. Ji, B. Zhang, M. Chen, X. Wu, Y. Zhu, X. Yu, J. Wang, H. Zhang, Y. Hong, Y. Zou, G. Feng, Y. Qiao, H. Zhou, S. G. Sun, Angew. Chem. Int. Ed. Engl. **2024**, 63, e202412214.
[40] Y. Lu, C.-Z. Zhao, J.-Q. Huang, Q. Zhang, Joule. **2022**, 6, 1172–1198.

View Article Online
DOI: 10.1039/D6SC02973F

The data that support the findings of this study are available from the corresponding author upon reasonable request.